The BEM-FDM model of thermal processes proceeding in the domain of the human finger

Ewa Majchrzak[1], Bohdan Mochnacki[2], Damian Tarasek[3], Mirosław Dziewoński[1]*

[1] Silesian University of Technology, Gliwice, Poland.
[2] Higher School of Labour Safety Management, Katowice, Poland.
[3] Manchester Metropolitan University, Manchester, UK.

Purpose: The problem of the numerical modeling of thermal processes proceeding in the non-homogeneous domain of the human finger is discussed. The domain considered constitutes the assembling of soft and bone tissues and the system of supplying blood vessels (arteries and veins). The mathematical description of the process analyzed corresponds to the so-called vascular models. Methods: At the stage of numerical modeling the algorithm being the composition of the boundary element method (BEM) and the finite difference method (FDM) is applied. Results: The algorithm presented allows one to determine the steady state temperature field in the finger domain in natural convection conditions. To verify the effectiveness and exactness of the method of the problem solution, the thermal imaging measurements of the finger surface temperature have been done. Conclusions: The compatibility of numerical and experimental results (the natural convection conditions) has proved to be quite satisfactory. It is possible to use the algorithm proposed for the modeling of thermal processes proceeding in the conditions of low or high ambient temperatures and the big values of heat transfer coefficients. The impact of protective clothing on the temperature field in the domain of the finger can also be analyzed.

Key words: *bioheat transfer, boundary element method, countercurrent blood flow, thermograms*

1. Introduction

Mathematical models connected with the description of thermal processes proceeding in the human finger can be divided into two groups. The first group is associated with the bioheat modeling of whole human body to predict skin and core segmental temperatures using physiology and thermoregulatory functions [7], [21]. In such models the human body is divided into the different numbers of segments of varied shapes and dimensions and the thermal interactions between the segments are in different ways taken into account. The first multisegmental model of human body was presented by Stolwijk [29]. In this model, the human body is divided into cylinders: trunk, arms, hands, legs, feet and a spherical head. In each segment four concentric layers corresponding to the core, muscle, fat and skin tissue are distinguished. The segments are connected through blood flow in the arteries and veins and the appropriate thermal control equations are formulated. In the more complex model presented by Wissler [31] the human body consists of fifteen cylindrical segments, while in the Fiala model [3] the body is represented by fifteen spherical or cylindrical elements (head, face, neck, shoulders, arms, hands, thorax, abdomen, legs and feet). The idea of division of the human body into sectors was applied many times by different researchers as well. For example, in paper [22], the most accurate and realistic representation of the arterial system including blood flow pulsation is presented and clothing model is introduced. In work [4], the elliptical cylinders are used to represent the body segments and eight types of tissues are considered: skin, fat, muscle, bone, viscera, lung, heart, and brain. In paper [23], the hemodynamic model which is an enhanced version of the Avolio model [1] coupled with the circle of Willis [32] is presented and it allows one to provide detailed information on perfu-

sion of the inner organs and the brain. The authors of paper [30] are presenting a more realistic human thermal model and they use shaped and refined body segments to simulate heat and mass transfer in the human body during a transient process. In paper [24], the digital thermal monitoring based on the response of finger temperature to vessel occlusion and reperfusion is presented and a real geometric model of human hand integrated with the hemodynamic model of blood circulation in upper limb is developed.

The second group allows one to model the finger as independent segment from the body but it requires empirical inputs on the arterial and venous blood flow. In this place, papers [25], [26] should be mentioned. The authors analyze the thermal processes proceeding in the finger domain subjected to the different environmental conditions (the transient problem has been considered). Taking into account countercurrent arterio-venous heat exchange the similar local models have been developed by, e.g., Stańczyk and Telega [27], Majchrzak and Mochnacki [9], [11].

This paper is intended to propose the numerical model of heat exchange between the single human finger and environment proceeding in the conditions of natural convection (a steady state problem) and belongs to the second group of the models mentioned above. The algorithm presented allows one to consider the different conditions on the external surface of the system. In the domain considered the sub-domains of bone tissue and soft tissue are distinguished. The finger domain is powered by the pairs of blood vessels (artery and vein – the countercurrent flow is taken into account). The thermal effects of the small vessels action are included in the Pennes equation [20] concerning the soft tissue sub-domain (a perfusion heat source). From a mathematical point of view the model of the process is created by the system of PDE determining the temperature distribution in the sub-domains of tissue and the ordinary differential equations describing the blood temperature changes along the vessels. It should be pointed out that the equations describing blood temperature are based on the model presented in [9]. In this paper, the tissue and vascular models are coupled by the conditions resulting from the continuity of the boundary heat flux, additionally a certain iterative procedure must be taken into account. At the stage of numerical computations the hybrid algorithm using the boundary element method (a tissue model) and the finite difference method (a vascular model) has been applied.

The results obtained have been compared with the measurements of temperature distribution on the finger surface done using thermal imaging techniques.

2. Material and methods

The real geometry of the human finger is approximated by the cylinder with dimensions R (radius) and $Z + L$ (height), at the same time the sub-domains of bone tissue (cylinder of radius R_c) and soft tissue are taken into account. The domain considered is powered by the four pairs of vessels (artery and vein). The cylindrical domain of the soft tissue located in the lower part of the system corresponds to the fingertip (Fig. 1).
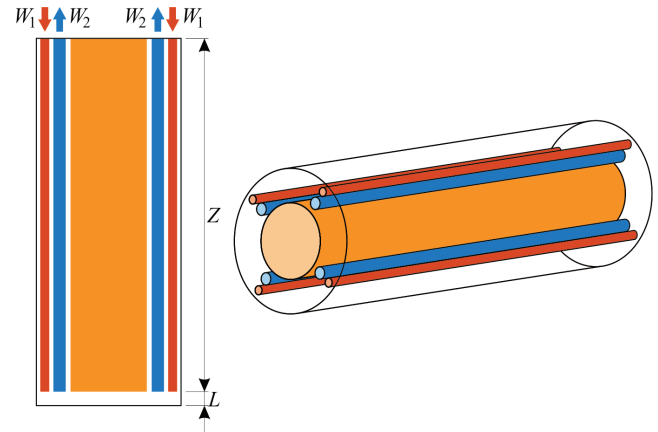

Fig. 1. Domain considered

The steady temperature field $T(x_1, x_2, z)$ in domain of soft tissue is described by the Pennes equation

$$(x_1, x_2, z) \in \Omega_z: \ \lambda \nabla^2(x_1, x_2, z)$$
$$+ G_B c_B \rho_B [T_B - T(x_1, x_2, z)] + Q_{met} = 0 \qquad (1)$$

where λ is the thermal conductivity of tissue, c_B is the specific heat of blood, ρ_B is the blood density, G_B [1/s] is the perfusion coefficient, T_B is the blood temperature in the capillaries, Q_{met} is the metabolic heat source, T, x_1, x_2, z denote temperature and geometrical co-ordinates.

The temperature field $T_c(x_1, x_2, z)$ in domain of bone tissue is described by the Laplace equation, namely,

$$(x_1, x_2, z) \in \Omega_c: \ \lambda_c \nabla^2 T_c(x_1, x_2, z) = 0 \qquad (2)$$

where λ_c is the bone tissue thermal conductivity.

On the contact surface between sub-domains considered the continuity of heat flux and temperature is assumed

$$(x_1, x_2, z) \in \Gamma_c:$$
$$\begin{cases} -\lambda \mathbf{n} \cdot \nabla T(x_1, x_2, z) = -\lambda_c \mathbf{n} \cdot \nabla T_c(x_1, x_2, z) \\ T(x_1, x_2, z) = T_c(x_1, x_2, z) \end{cases} \qquad (3)$$

where $\mathbf{n} \cdot \nabla T(x_1, x_2, z)$ is the normal derivative.

On the contact surface between soft tissue and vessels the well known Robin conditions can be accepted

$$(x_1, x_2, z) \in \Gamma_1 : \begin{aligned} q(x_1, x_2, z) = -\lambda \mathbf{n} \cdot \nabla T(x_1, x_2, z) = \\ \alpha_1 [T(x_1, x_2, z) - T_{B1}(z)], \end{aligned}$$

$$(x_1, x_2, z) \in \Gamma_2 : \begin{aligned} q(x_1, x_2, z) = -\lambda \mathbf{n} \cdot \nabla T(x_1, x_2, z) = \\ \alpha_2 [T(x_1, x_2, z) - T_{B2}(z)] \end{aligned} \tag{4}$$

where Γ_1 are the surfaces between arteries and tissue (Γ_{11}, Γ_{12}, Γ_{13}, Γ_{14}, Fig. 2), Γ_2 are the surfaces between veins and tissue (Γ_{21}, Γ_{22}, Γ_{23}, Γ_{24}), $T_{B1}(z)$, $T_{B2}(z)$ are the arterial and venous blood temperatures, α_1 and α_2 are the heat transfer coefficients. It should be pointed out that artery and vein radiuses are different.

On the outer surface of the system there is assumed the boundary condition in the form

$$(x_1, x_2, z) \in \Gamma_0 : q(x_1, x_2, z) = -\lambda \mathbf{n} \cdot \nabla T(x_1, x_2, z)$$
$$= \alpha [T(x_1, x_2, z) - T_a] \tag{5}$$

where α is the heat transfer coefficient, T_a is the ambient temperature.
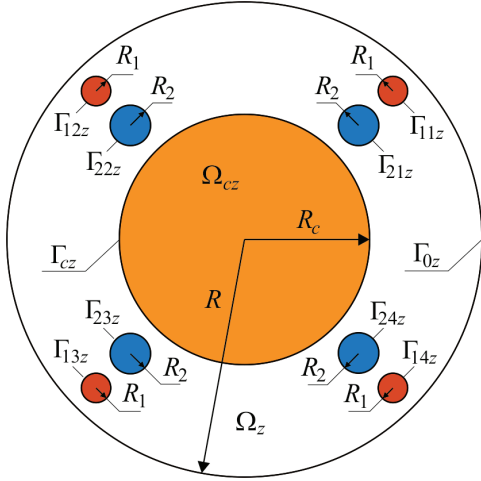

Fig. 2. The cross-section of the system

The temperature distribution along the vessels is described by the following equations (the detailed considerations of these equations can be found in [9], [15])

$$\frac{dT_{B1}(z)}{dz} = \frac{2\alpha_1}{w_1 c_B \rho_B R_1} [T_{v1}(z) - T_{B1}(z)] + \frac{Q_{Bmet}}{w_1 c_B \rho_B} \tag{6}$$

and

$$\frac{dT_{B2}(z)}{dz} = \frac{2\alpha_2}{w_2 c_B \rho_B R_2} [T_{v2}(z) - T_{B2}(z)] + \frac{Q_{Bmet}}{w_2 c_B \rho_B} \tag{7}$$

where w_1, w_2 are the blood velocities in arteries and veins, T_{v1}, T_{v2} are the mean blood vessel wall temperatures corresponding to co-ordinate z, R_1, R_2 are the radiuses of arteries and veins. The last equations are supplemented by the initial conditions $T_{B1}(0) = T_{B10}$ and $T_{B2}(Z) = T_{B20}$.

The above-formulated problem has been solved using the hybrid iterative algorithm that is submission of the BEM and FDM. In particular, the multiple reciprocity BEM [8], [18], [19] is applied for the soft tissue sub-domain (because of the non-zero value of source function), the classical variant of the BEM (e.g., [2]) for bone tissue sub-domain and the FDM (the Euler method) for the vessels sub-domains.

Let us assume that the temperature field in the cross section z = const. in the domain considered (Fig. 2) is described by the following equations
– for soft tissue

$$x \in \Omega_z : \ \lambda \nabla^2 T(x) + G_B c_B \rho_B T(x) + Q = 0, \quad x = \{x_1, x_2\} \tag{8}$$

where

$$Q = G_B c_B \rho_B T + Q_{met}, \tag{9}$$

– for bone tissue

$$x \in \Omega_c : \ \lambda_c \nabla^2 T_c(x) = 0, \quad x = \{x_1, x_2\}. \tag{10}$$

Equations (8) and (10) are supplemented by the boundary conditions

$$x \in \Gamma_{1z} : q(x) = -\lambda \mathbf{n} \cdot \nabla T(x) = \alpha_1 [T_{v1}(z) - T_{B1}(z)],$$

$$x \in \Gamma_{2z} : q(x) = -\lambda \mathbf{n} \cdot \nabla T(x) = \alpha_2 [T_{v2}(z) - T_{B2}(z)], \tag{11}$$

$$x \in \Gamma_{0z} : q(x) = -\lambda \mathbf{n} \cdot \nabla T(x) = \alpha [T(x) - T_a],$$

and

$$x \in \Gamma_{cz} : \begin{cases} q(x) = -q_c(x), \\ T(x) = T_c(x). \end{cases} \tag{12}$$

One can see that the heat conduction in z direction is omitted here. This assumption is confirmed by the course of the real process. The multiple reciprocity BEM for the problem described by equation (8) leads to the following integral equation [19]

$$B(\xi)T(\xi) + \sum_{l=0}^{\infty} \left(\frac{G_B c_B \rho_B}{\lambda} \right)^l \int_{\Gamma_z} q(x) V_l^*(\xi, x) d\Gamma_z$$

$$= \sum_{l=0}^{\infty} \left(\frac{G_B c_B \rho_B}{\lambda} \right)^l \int_{\Gamma_z} T(x) Z_l^*(\xi, x) d\Gamma_z$$

$$- \frac{Q}{\lambda} \sum_{l=1}^{\infty} \left(\frac{G_B c_B \rho_B}{\lambda} \right)^{l-1} \int_{\Gamma_z} Z_l^*(\xi, x) d\Gamma_z \tag{13}$$

where ξ is the observation point, $B(\xi) \in (0, 1]$. The coefficient $B(\xi)$ is dependent on the location of source point ξ. For all the points located inside the domain Ω_z the coefficient $B(\xi) = 1$. When the point ξ belongs to the boundary $\Gamma_z = \Gamma_{1z} \cup \Gamma_{2z} \cup \Gamma_{0z} \cup \Gamma_{cz}$ then this coefficient is equal to $\beta/2\pi$, where β is the internal angle which the boundary makes at point ξ.

Functions $V_l^*(\xi, x)$ are defined as follows

$$V_l^*(\xi, x) = \frac{1}{2\pi\lambda} r^{2l} \left(A_l \ln\frac{1}{r} + B_l \right) \qquad (14)$$

where r is the distance between the points ξ and x, while

$$\begin{array}{llll} A_0 = 1, & A_l = \dfrac{A_{l-1}}{4l^2}, & & l = 1, 2, 3, \dots \\[2mm] B_0 = 0, & B_l = \dfrac{1}{4l^2}\left(\dfrac{A_{l-1}}{l} + B_{l-1} \right), & & l = 1, 2, 3, \dots \end{array} \qquad (15)$$

In equation (13), $q(x) = -\lambda\mathbf{n}\cdot\nabla T(x)$ is the boundary heat flux and $Z_l^*(\xi, x) = -\lambda\mathbf{n}\cdot V_l^*(\xi, x)$.

The functions $Z_l^*(\xi, x)$ can be calculated analytically and then

$$Z_l^*(\xi, x) = \frac{d}{2\pi} r^{2l-2}\left[A_l - 2l\left(A_l \ln\frac{1}{r} + B_l \right) \right] \quad (16)$$

where

$$d = (x_1 - \xi_1)\cos\alpha_1 + (x_2 - \xi_2)\cos\alpha_2, \qquad (17)$$

while $\cos\alpha_1$, $\cos\alpha_2$ are the directional cosines of the normal outward vector $\mathbf{n}$.

It should be pointed out that in order to solve the boundary integral equation (13) the discretization of the boundary should be introduced (Fig. 3) and the adequate series must be convergent [19]. So, the boundary Γ_z of soft tissue is divided into N boundary elements Γ_j, $j = 1, 2, \dots, N$. Next, the integrals in equation (13) are substituted by the sums of integrals over these elements

$$B(\xi^i)T(\xi^i) + \sum_{l=0}^{\infty}\left(\frac{G_B c_B}{\lambda} \right)^l \sum_{j=1}^{N} \int_{\Gamma_j} q(x)V_l^*(\xi^i, x)d\Gamma_j$$

$$= \sum_{l=0}^{\infty}\left(\frac{G_B c_B}{\lambda} \right)^l \sum_{j=1}^{N} \int_{\Gamma_j} T(x)Z_l^*(\xi^i, x)d\Gamma_j$$

$$- \frac{Q}{\lambda}\sum_{l=0}^{\infty}\left(\frac{G_B c_B}{\lambda} \right)^l \sum_{j=1}^{N} \int_{\Gamma_j} Z_{l+1}^*(\xi^i, x)d\Gamma_j. \qquad (18)$$

In this paper, the parabolic boundary elements are applied and finally one obtains the following system of algebraic equations

$$\sum_{k=1}^{K} G_{ik}q_{ik} = \sum_{k=1}^{K} H_{ik}T_k + \sum_{k=1}^{K} P_{ik}, \quad i = 1, 2, 3, \dots, K \quad (19)$$

or using the matrix convention

$$\mathbf{Gq} = \mathbf{HT} + \mathbf{P} \qquad (20)$$

where K is the number of boundary nodes. The way of computing G_{ik}, H_{ik} and P_{ik} is described in detail in [18], [11], [16].

To solve equation (10) describing the temperature distribution in the bone tissue sub-domain the classical variant of the BEM for elliptic equation [2] has been used, and then

$$B(\xi)T_c(\xi) + \int_{\Gamma_{cz}} T_c^*(\xi, x)q_c(x)d\Gamma_{cz}$$

$$= \int_{\Gamma_{cz}} q_c^*(\xi, x)T_c(x)d\Gamma_{cz} \qquad (21)$$

where

$$T_c^*(\xi, x) = \frac{1}{2\pi\lambda_c} \ln\frac{1}{r} \qquad (22)$$

is the fundamental solution, while

$$q_c^*(\xi, x) = \frac{d}{2\pi r} \qquad (23)$$

is an analogue of heat flux resulting from the fundamental solution, r is the distance between the points ξ and x, d is described by formula (17).

As previously stated, the parabolic boundary elements have been used and for bone tissue sub-domain one obtains the following system of equations

$$\sum_{k=K+1}^{K_c} G_{ik}^c q_k^c = \sum_{k=K+1}^{K_c} H_{ik}^c T_k^c, \quad i = K+1, K+2, \dots, K_c \quad (24)$$

or

$$-\sum_{k=K+1}^{K_c} H_{ik}^c T_k^c + \sum_{k=K+1}^{K_c} G_{ik}^c q_k^c = 0, \quad i = K+1, K+2, \dots, K_c. \qquad (25)$$

Using the matrix form one has

$$-\mathbf{H}^c\mathbf{T}^c + \mathbf{G}^c\mathbf{q}^c = 0. \qquad (26)$$

The way of calculating G_{ik}^c, H_{ik}^c is described, among others, in [2]. It should be pointed out that in system (25) both the boundary temperatures and the boundary heat fluxes are unknown.
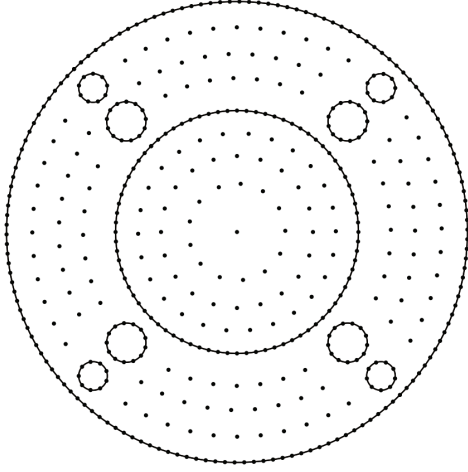
Fig. 3. Boundary and internal nodes

In system (19), the components concerning the successive parts of the boundary should be separated, i.e.,

$$\sum_{k=1}^{K_1} G_{ik} q_k + \sum_{k=K_1+1}^{K_1+K_2} G_{ik} q_k + \sum_{k=K_1+K_2+1}^{K_3} G_{ik} q_k$$

$$+ \sum_{k=K_1+K_2+K_3+1}^{K} G_{ik} q_k = \sum_{k=1}^{K_1} H_{ik} T_k + \sum_{k=K_1+1}^{K_1+K_2} H_{ik} T_k$$

$$+ \sum_{k=K_1+K_2+1}^{K_3} H_{ik} T_k + \sum_{k=K_1+K_2+K_3+1}^{K} H_{ik} T_k + \sum_{k=1}^{K} P_{ik} \quad (27)$$

where K_1 is the number of nodes located on the external boundary Γ_{0z}, K_2 is the number of nodes located on the boundary Γ_{cz} between soft and bone tissue, K_3 and $K_4 = K - (K_1 + K_2 + K_3)$ are the numbers of nodes located on the vessel walls (arteries and veins, respectively). Taking into account the boundary conditions assumed, the system of equations (27) can be written in the form

$$\sum_{k=1}^{K_1} G_{ik} \alpha (T_k - T_a) + \sum_{k=K_1+1}^{K_1+K_2} G_{ik} q_k$$

$$+ \sum_{k=K_1+K_2+1}^{K_3} G_{ik} \alpha_1 [T_k - T_{B1}(z)]$$

$$+ \sum_{k=K_1+K_2+K_3+1}^{K} G_{ik} \alpha_2 [T_k - T_{B2}(z)]$$

$$= \sum_{k=1}^{K_1} H_{ik} T_k + \sum_{k=K_1+1}^{K_1+K_2} H_{ik} T_k$$

$$+ \sum_{k=K_1+K_2+1}^{K_3} H_{ik} T_k + \sum_{k=K_1+K_2+K_3+1}^{K} H_{ik} T_k + \sum_{k=1}^{K} P_{ik} \quad (28)$$

or

$$\sum_{k=1}^{K_1} (\alpha G_{ik} - H_{ik}) T_k - \sum_{k=K_1+1}^{K_1+K_2} H_{ik} T_k$$

$$+ \sum_{k=K_1+1}^{K_1+K_2} G_{ik} q_k + \sum_{k=K_1+K_2+1}^{K_3} (\alpha_1 G_{ik} - H_{ik}) T_k$$

$$+ \sum_{k=K_1+K_2+K_3+1}^{K} (\alpha_2 G_{ik} - H_{ik}) T_k$$

$$= \sum_{k=1}^{K_1} (\alpha G_{ik} T_a + \sum_{k=K_1+K_2+1}^{K_3} \alpha_1 G_{ik} T_{B1}(z)$$

$$+ \sum_{k=K_1+K_2+K_3+1}^{K} \alpha_2 G_{ik} T_{B2}(z) + \sum_{k=1}^{K} P_{ik}. \quad (29)$$

Let us introduce the following denotations

$$\mathbf{T}^1 = \begin{bmatrix} T_1 \\ ... \\ T_{K_1} \end{bmatrix}, \quad \mathbf{T}^2 = \begin{bmatrix} T_{K_1+1} \\ ... \\ T_{K_1+K_2} \end{bmatrix},$$

$$\mathbf{T}^3 = \begin{bmatrix} T_{K_1+K_2+1} \\ ... \\ T_{K_1+K_2+K_3} \end{bmatrix}, \quad \mathbf{T}^4 = \begin{bmatrix} T_{K_1+K_2+K_3+1} \\ ... \\ T_K \end{bmatrix} \quad (30)$$

and

$$\mathbf{q}^1 = \begin{bmatrix} q_1 \\ ... \\ q_{K_1} \end{bmatrix}, \quad \mathbf{q}^2 = \begin{bmatrix} q_{K_1+1} \\ ... \\ q_{K_1+K_2} \end{bmatrix},$$

$$\mathbf{q}^3 = \begin{bmatrix} q_{K_1+K_2+1} \\ ... \\ q_{K_1+K_2+K_3} \end{bmatrix}, \quad \mathbf{q}^4 = \begin{bmatrix} q_{K_1+K_2+K_3+1} \\ ... \\ q_K \end{bmatrix}. \quad (31)$$

As can be seen, the successive vectors correspond to the values of temperatures and heat fluxes on the external and internal boundaries and the walls of vessels.

Additionally, we denote

$$\mathbf{G}^1 = \begin{bmatrix} G_{11} & ... & G_{1K_1} \\ ... & ... & K \\ G_{K1} & ... & G_{KK_1} \end{bmatrix},$$

$$\mathbf{G}^2 = \begin{bmatrix} G_{1,K_1+1} & ... & G_{1,K_1+K_2} \\ ... & ... & ... \\ G_{K,K_1+1} & ... & G_{K,K_1+K_2} \end{bmatrix}, \quad (32)$$

$$\mathbf{G}^3 = \begin{bmatrix} G_{1,K_1+K_2+1} & ... & G_{1,K_1+K_2+K_3} \\ ... & ... & ... \\ G_{K,K_1+K_2+1} & ... & G_{K,K_1+K_2+K_3} \end{bmatrix},$$

$$\mathbf{G}^4 = \begin{bmatrix} G_{1,K_1+K_2+K_3+1} & \cdots & G_{1,K} \\ \cdots & \cdots & \cdots \\ G_{K,K_1+K_2+K_3+1} & \cdots & G_{K,K} \end{bmatrix}, \quad (32)$$

$$\mathbf{H}^1 = \begin{bmatrix} H_{11} & \cdots & H_{1K_1} \\ \cdots & \cdots & \cdots \\ H_{K1} & \cdots & H_{KK_1} \end{bmatrix},$$

$$\mathbf{H}^2 = \begin{bmatrix} H_{1,K_1+1} & \cdots & H_{1,K_1+K_2} \\ \cdots & \cdots & \cdots \\ H_{K,K_1+1} & \cdots & H_{K,K_1+K_2} \end{bmatrix},$$

$$(33)$$

$$\mathbf{H}^3 = \begin{bmatrix} H_{1,K_1+K_2+1} & \cdots & H_{1,K_1+K_2+K_3} \\ \cdots & \cdots & \cdots \\ H_{K,K_1+K_2+1} & \cdots & H_{K,K_1+K_2+K_3} \end{bmatrix},$$

$$\mathbf{H}^4 = \begin{bmatrix} H_{1,K_1+K_2+K_3+1} & \cdots & H_{1,K} \\ \cdots & \cdots & \cdots \\ H_{K,K_1+K_2+K_3+1} & \cdots & H_{K,K} \end{bmatrix},$$

These rectangular matrices are extracted from the matrices $\mathbf{G}$ and $\mathbf{H}$, namely,

$$\mathbf{G} = [\mathbf{G}^1 \ \mathbf{G}^2 \ \mathbf{G}^3 \ \mathbf{G}^4], \quad \mathbf{H} = [\mathbf{H}^1 \ \mathbf{H}^2 \ \mathbf{H}^3 \ \mathbf{H}^4]. \quad (34)$$

So, the system of equations (29) can be written in the form

$$[\alpha\mathbf{G}^1 - \mathbf{H}^1 \quad -\mathbf{H}^2 \quad \mathbf{G}^2 \quad \alpha_1\mathbf{G}^3 - \mathbf{H}^3 \quad \alpha_2\mathbf{G}^4 - \mathbf{H}^4]$$

$$\times \begin{bmatrix} \mathbf{T}^1 \\ \mathbf{T}^2 \\ \mathbf{q}^2 \\ \mathbf{T}^3 \\ \mathbf{T}^4 \end{bmatrix} = [\alpha\mathbf{G}^1\mathbf{T}_a + \alpha_1\mathbf{G}^3\mathbf{T}_{B1} + \alpha_2\mathbf{G}^4\mathbf{T}_{B2} + \mathbf{P}] \quad (35)$$

where

$$\mathbf{T}_{B1} = \begin{bmatrix} T_{B1}(z) \\ \cdots \\ T_{B1}(z) \end{bmatrix}, \quad \mathbf{T}_{B2} = \begin{bmatrix} T_{B2}(z) \\ \cdots \\ T_{B2}(z) \end{bmatrix}, \quad \mathbf{T}_a = \begin{bmatrix} T_a \\ \cdots \\ T_a \end{bmatrix} \quad (36)$$

The number of the above vector components corresponds to the number of columns of the matrices $\mathbf{G}^1$, $\mathbf{G}^2$, $\mathbf{G}^3$ and $\mathbf{G}^4$ (similarly $\mathbf{H}^1$, $\mathbf{H}^2$, $\mathbf{H}^3$ and $\mathbf{H}^4$).

Now, to the systems of equations (35) and (26) the boundary condition (12) written in the form

$$x \in \Gamma_{cz}: \begin{cases} \mathbf{T}^2 = \mathbf{T}^c = \mathbf{T}, \\ \mathbf{q}^2 = -\mathbf{q}^c = \mathbf{q}, \end{cases} \quad (37)$$

is introduced and then the coupling of the above systems gives

$$\begin{bmatrix} \alpha\mathbf{G}^1 - \mathbf{H}^1 & -\mathbf{H}^2 & \mathbf{G}^2 & \alpha_1\mathbf{G}^3 - \mathbf{H}^3 & \alpha_2\mathbf{G}^4 - \mathbf{H}^4 \\ \mathbf{0} & -\mathbf{H}^c & -\mathbf{G}^c & \mathbf{0} & \mathbf{0} \end{bmatrix}$$

$$\times \begin{bmatrix} \mathbf{T}^1 \\ \mathbf{T} \\ \mathbf{q} \\ \mathbf{T}^3 \\ \mathbf{T}^4 \end{bmatrix} = \begin{bmatrix} \alpha\mathbf{G}^1\mathbf{T}_a + \alpha_1\mathbf{G}^3\mathbf{T}_{B1} + \alpha_2\mathbf{G}^4\mathbf{T}_{B2} + \mathbf{P} \\ \mathbf{0} \end{bmatrix}. \quad (38)$$

The solution of equation (38) allows one to determine heat fluxes

– at the nodes located on the walls of arteries

$$\mathbf{q}^3 = \alpha_1(\mathbf{T}^3 - \mathbf{T}_{B1}), \quad (39)$$

– at the nodes located on the walls of veins

$$\mathbf{q}^4 = \alpha_2(\mathbf{T}^4 - \mathbf{T}_{B2}), \quad (40)$$

– at the nodes located on the external surface

$$\mathbf{q}^1 = \alpha(\mathbf{T} - \mathbf{T}_a). \quad (41)$$

The last stage comes down to computations of temperatures at the internal nodes from the subdomain of the soft tissue

$$T_i = \sum_{k=1}^{K} H_{ik}T_k - \sum_{k=1}^{K} G_{ik}q_k + \sum_{k=1}^{K} P_{ik} \quad (42)$$

and at the internal nodes of bone tissue

$$T_i^c = \sum_{k=K+1}^{K_c} H_{ik}^c T_k^c - \sum_{k=K+1}^{K_c} G_{ik}^c q_k^c. \quad (43)$$

Internal nodes (as in Fig. 3) are introduced only in order to present the temperature distribution in the successive sections. So, the algorithm proposed belongs to the group of meshless methods.

The next step of computations (transition to the successive cross-section $z + \Delta z$) requires the averaging of the temperatures of vessel walls within each of the blood vessels (see equations (6) and (7)).

The blood temperatures (artery and vein) can be found using the equations

$$T_{B1}(z + \Delta z) = (1 - A_1\Delta z)T_{B1}(z) + A_1\Delta z T_{v1}(z) + B_1\Delta z \quad (44)$$

and

$$T_{B2}(z + \Delta z) = (1 + A_2\Delta z)T_{B2}(z) - A_1\Delta z T_{v2}(z) - B_2\Delta z \quad (45)$$

where

$$A_e = \frac{2\alpha_e}{w_e c_B \rho_B R_e}, \quad B_e = \frac{Q_{Bmet}}{w_e c_B \rho_B}, \quad e = 1, 2, \quad (46)$$

while $T_{v1}(z)$ and $T_{v2}(z)$ are the averaged temperatures of the vessel walls.

The idea of the algorithm proposed is the following. For the cross-section $z = 0$ and arbitrary assumed temperature $T_{B2}(0)$ (the temperature $T_{B1}(0) = T_{B10}$ is known from the initial condition, of course) the system of equations (38) is solved. Next, the mean values of the temperatures of vessel walls are calculated

$$T_{v1}(z) = \frac{1}{K_3} \sum_{k=K_1+K_2+1}^{K_3} T_k, \quad T_{v2}(z) = \frac{1}{K_4} \sum_{k=K_1+K_2+K_3+1}^{K} T_k.$$
$$(47)$$

Putting $z = 0$ in equations (44) and (45) the temperatures $T_{B1}(\Delta z)$ and $T_{B2}(\Delta z)$ are calculated and these values are introduced to the system of equations (38). From this system of equations the boundary temperatures for cross section $z = \Delta z$ are determined. The mean values of vessel wall temperatures are determined from (47), next using the formulas (44), (45)

Fig. 4. Flowchart

the blood temperatures $T_{B1}(2\Delta z)$ and $T_{B2}(2\Delta z)$ can be found. These temperatures introduced to the system of equations (38) allow one to calculate the boundary temperatures for the cross section $2\Delta z$. The procedure is continued until the cross section $z = Z$ is achieved. If $T_{B2}(Z) \neq T_{B20}$ then the procedure is repeated for the other value of $T_{B2}(0)$. The iteration process is continued until the calculated value $T_{B2}(Z)$ is close to the temperature T_{B20}. Figure 4 shows a block diagram illustrating the elements of the numerical algorithm.

The final stage of computations concerns the temperature distribution in the domain of the finger tip. This part of the finger corresponds to the cylinder shown in the lower part of Fig. 1. Taking into account the dimensions of cylinder ($L \ll R$) one can assume that the significantly overwhelming amount of heat is conducted in the z direction and the 3D problem is treated as a set of 1D problems concerning the sectors between the upper and lower surfaces of the domain considered. The starting points of segments correspond to the internal nodes distinguished in the cross-section $z = Z$. So, on the surface $z = Z + L$ the Robin condition is given (heat transfer coefficient is equal to α), while on the surface $z = Z$ the Dirichlet condition is known. In this way the problem is reduced to a set of 1D tasks in the form

$$Z < z < Z + L: \quad \lambda \frac{d^2 T(z)}{dz^2}$$
$$+ G_B c_B \rho_B [T_B - T(z)] + Q_{met} = 0 \quad (48)$$

with the boundary conditions

$$\begin{aligned} z = Z: & \quad T(z) = T_{Zj}, \\ z = Z + L: & \quad q(z) = \alpha[T(z) - T_a], \end{aligned} \quad (49)$$

where T_{Zj} are the known temperatures at the points resulting from the nodes position for $z = Z$ (Fig. 3). The problems (48), (49) can be solved analytically, of course.

3. Results

The following dimensions of the domain considered are assumed (Fig. 2): finger radius $R = 0.01$ m, finger length $Z+L = 0.08$ m, bone radius $R_c = 0.005$ m, artery radius $R_1 = 0.0005$ m, vein radius $R_2 = 0.00075$ m.

Thermophysical parameters of sub-domains are equal to [27], [28]: thermal conductivity of soft tissue $\lambda = 0.5$ W/(mK), thermal conductivity of bone tissue $\lambda_c = 2.21$ W/(mK), thermal conductivity of blood $\lambda_B =$
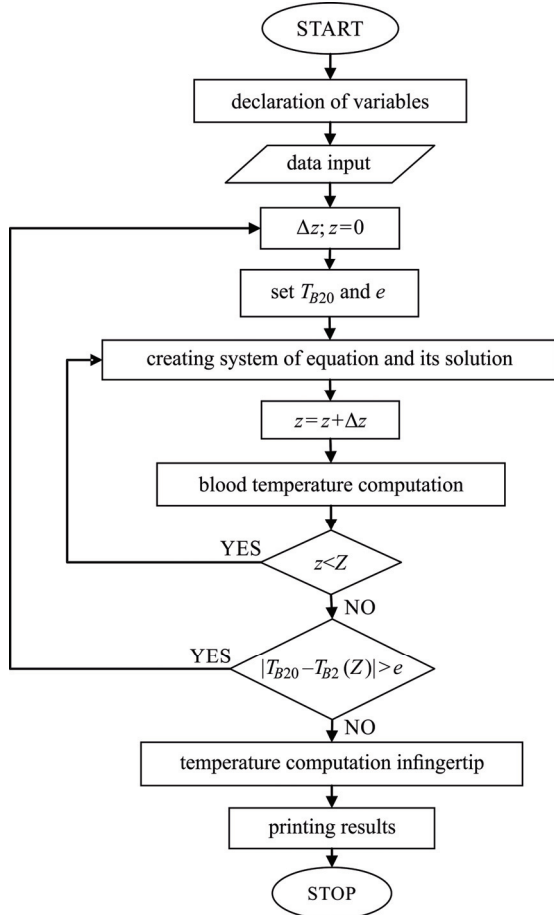
0.5 W/(mK), specific heat of blood c_B = 3770 J/(kgK), blood density ρ_B = 1060 kg/m^3, perfusion coefficient G_B = 0.0005425 1/s, metabolic heat sources Q_{met} = 245 W/m^3 and Q_{Bmet} = 100 W/m^3, blood temperature in the capillaries T_B = 28 °C. Additionally, the temperatures T_{B10} = 28.6 °C, T_{B20} = 26.4 °C are taken into account (see next section).

According to literature [6], the Nusselt and Peclet numbers are equal to Nu = 4 and Pe = 100. On the basis of this information one can determine α_1 = 2000 W/(m^{2}K), α_2 = 1333.33 W/(m^{2}K) and the blood rates w_1 = 0.0125 m/s, w_2 = 0.0083 m/s.

The external boundary of the cylinder cross-section is divided into 40 parabolic boundary elements containing 80 nodes (Fig. 3), on the boundary between soft and bone tissues the number of parabolic elements equals 20 (40 nodes). On the vessel walls 4 parabolic elements, 8 nodes (arteries) and 8 parabolic elements, 16 nodes (veins) are distinguished,

in other words (see equation (29)) K_1 = 80, K_2 = 40, K_3 = 4·8 = 32, K_4 = 4·16 = 64, K = 216. In z direction the step Δz = 0.001 m.

On the external surface of finger the heat transfer coefficient is equal to α = 10 W/(m^{2}K), while T_a = 21 °C.

In Figs. 5 and 6, the temperature distribution for the cross-sections corresponding to z = 0.02 m, 0.04 m, 0.06 m and 0.075 m is shown. As might be expected the solution obtained is symmetrical, which is a partial confirmation of the correctness of the numerical algorithm. The relatively large value of the bone tissue thermal conductivity causes that the temperature field in this sub-domain is close to the homogeneous one. The greatest temperature changes occur near the blood vessels. The artery and vein temperatures decrease in the z direction and near the finger tip equalize reaching the equilibrium value (see also Fig. 7).
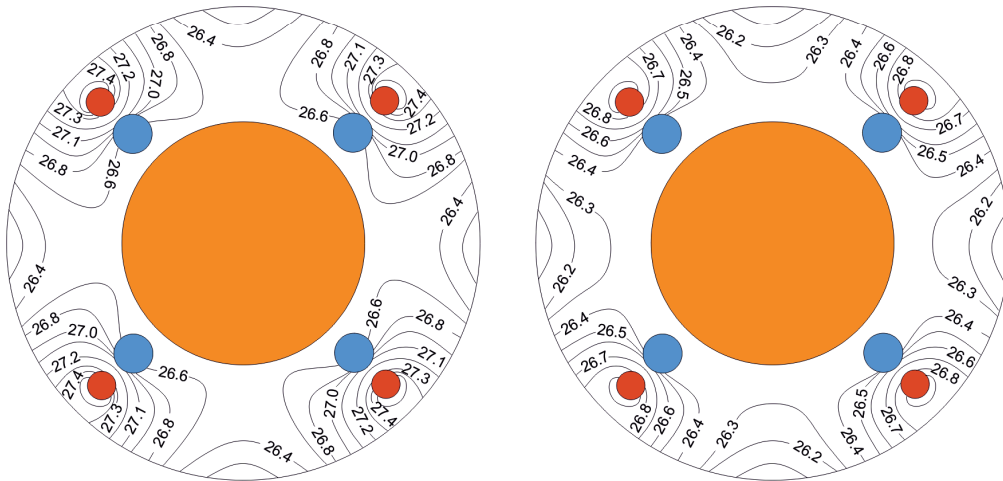

Fig. 5. Temperature distribution for z = 0.02 m and z = 0.04 m
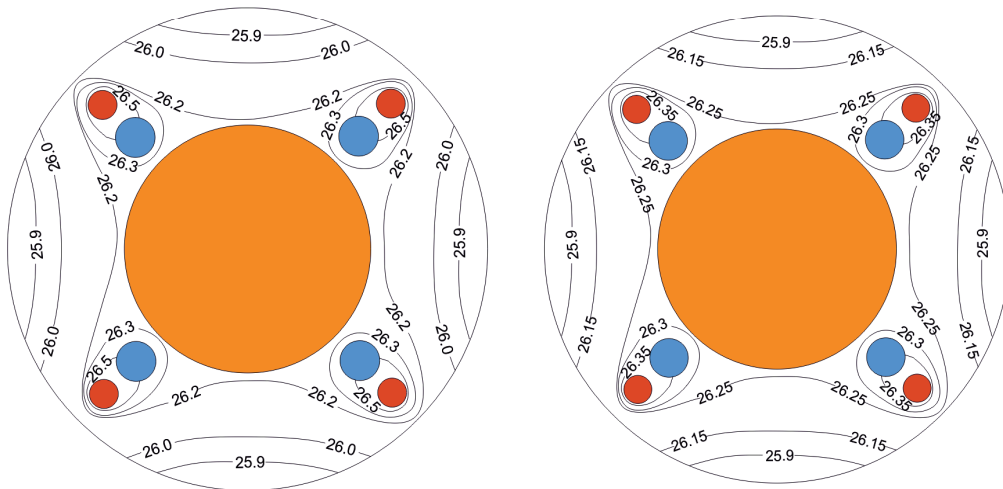

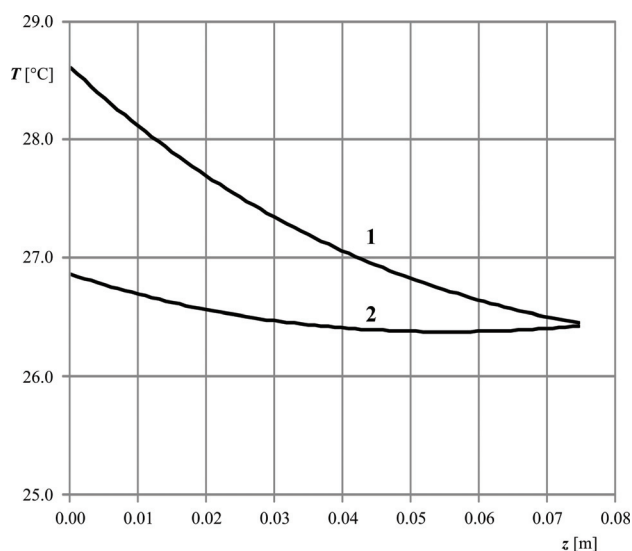Fig. 6. Temperature distribution for z = 0.06 m and z = 0.075 m

Fig. 7. Temperature distribution along the vessels:
1 – arteries, 2 – veins

In Fig. 8, the temperature distribution on the skin surface along *z* direction is shown. One can see that the skin surface temperatures at the points close to the regions of vessels are higher than the temperatures between the regions of vessels and their differences are clear. In the finger tip sub-domain the further decrease of temperature is explicitly visible.
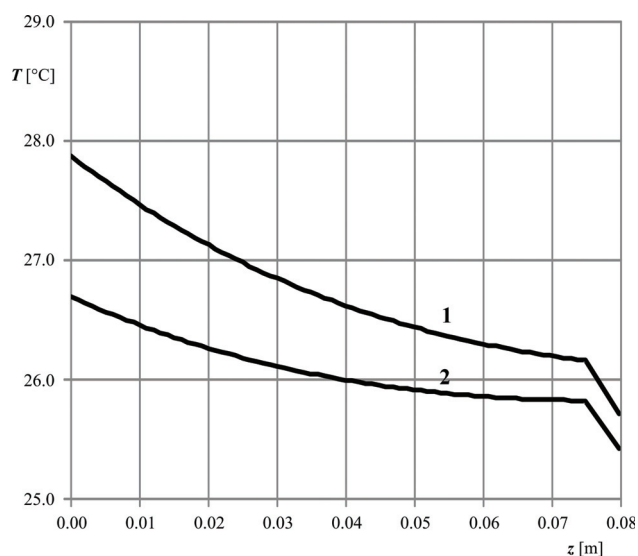

Fig. 8. Temperature distribution on the skin surface along *z* direction: 1 – close to the region of vessels, 2 – between the regions of vessels

4. Discussion

To confirm that the results are independent of the number of assumed boundary elements, the calculations

are repeated with doubled number of elements. In Fig. 9, a comparison of the results obtained for different number of elements is shown. The solid line represents the blood temperature distribution found for 216 boundary nodes, while the symbols the same distribution for 432 boundary nodes. The maximum temperature difference is equal to 0.02 K and is entirely acceptable.
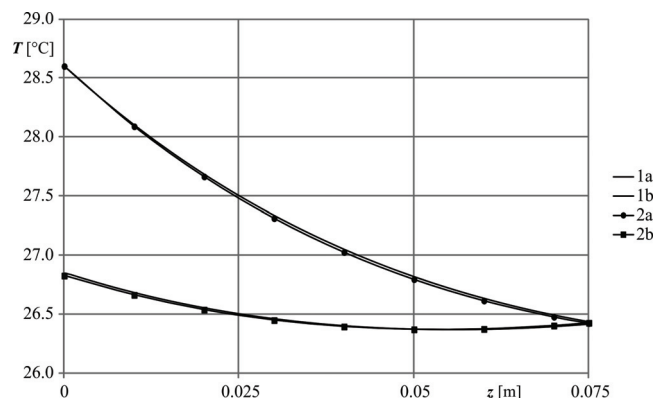

Fig. 9. Temperature distribution along the vessels for different numbers of boundary elements:
1 – arteries (1a – $K = 216$ boundary nodes, 1b – $K = 432$),
2 – veins (2a – $K = 216$, 2b – $K = 432$)

The numerical algorithm presented above should be verified experimentally because certain simplifying assumptions have been introduced and the vein temperature for $z = Z$ was adopted intuitively. Therefore, the thermograms of two volunteers have been done in the same external conditions ($\alpha = 5$ W/(m²K), $T_a = 20$ °C) and the results of measurements are shown in Figs. 10, 11 (hand) and in Figs. 12, 13 (change of temperature along the finger). As is well known the thermophysical parameters of biological tissue are varied and individualized (the same situation takes place in the case of finger geometry), so it is difficult to compare the results obtained (definitely harder than in the case of typical technical problems). For example, one can see the differences of surface temperature distribution visible in Figs. 10 and 11.

The results of computations and experiments are shown in Figs. 12 and 13. Calculations have been performed using the parameters given in the previous section, only the temperatures T_{B10} and T_{B20} were changed by means of the trial and error method. Results presented in Figs. 12 and 13 have been obtained under the assumption that for person I: $T_{B10} = 28.5$ °C, $T_{B20} = 26.8$ °C and for person II: $T_{B10} = 29.2$ °C, $T_{B20} = 26.2$ °C.

One can see that the courses of temperature profiles are similar, but the differences are visible.

Along the finger the skin surface temperature decreases by about 3 K. One can also observe a further temperature decrease at the tip region.
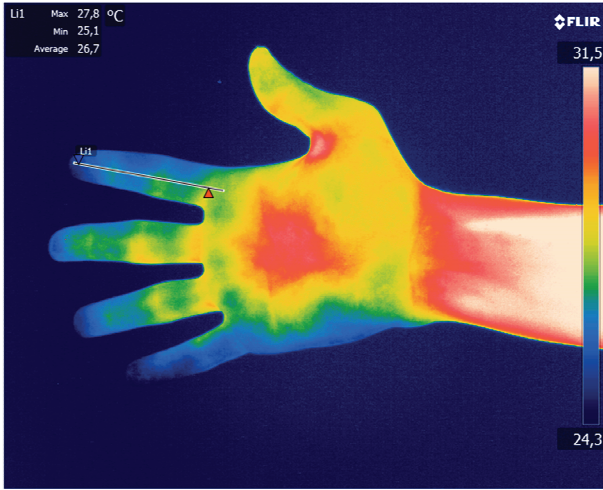
Fig. 10. Thermogram of the hand and measuring sector along the finger (person I)
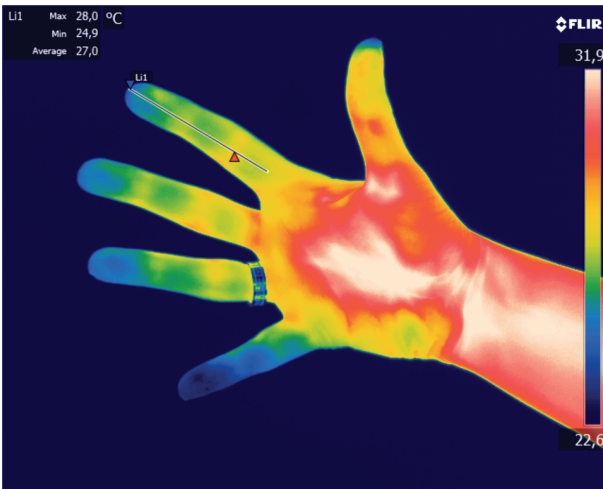

Fig. 11. Thermogram of the hand and measuring sector along the finger (person II)
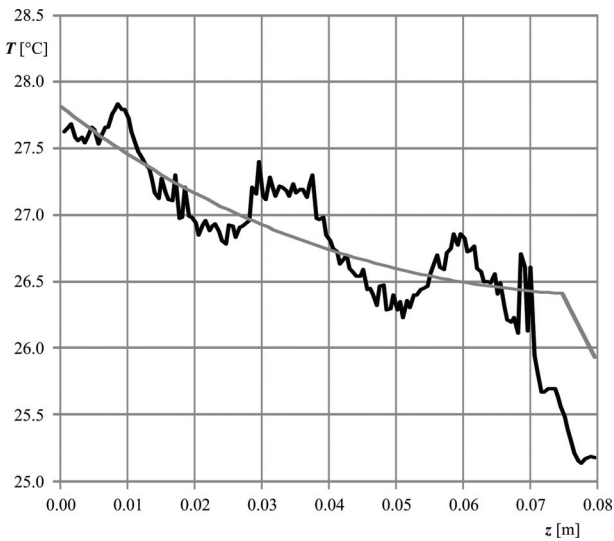

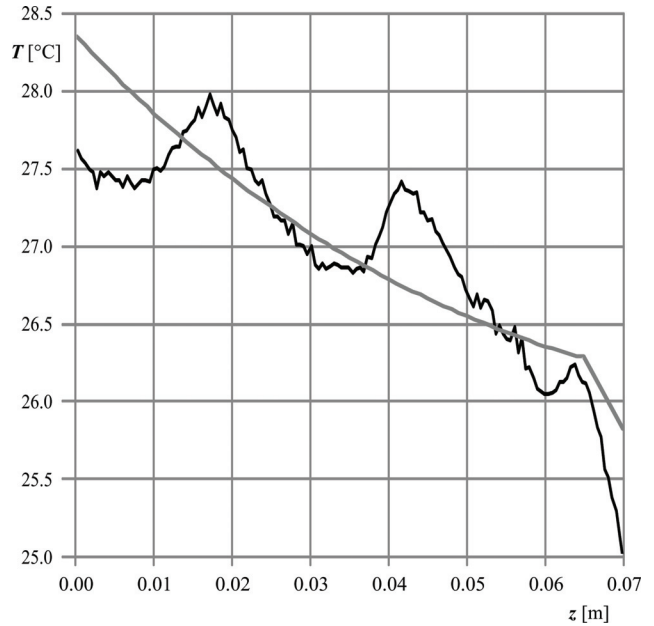Fig. 12. Comparison of measurements and calculated temperature (person I)

Fig. 13. Comparison of measurements and calculated temperature (person II)

A partial verification has been done by comparing the results obtained with the results presented in [5]. It should be pointed out that the comparison was only qualitative in nature because the mathematical model used in [5] is based on the theory of porous media and the way of presenting the results (dimensionless temperature) rather prevented a comparison of numerical values. But the general trends in temperature distributions are the same: the temperature of soft tissue surrounding the arteries is higher than the temperature of soft tissue surrounding the veins and the temperature on the skin surface along the finger from the basal part to the finger tip decreases.

It should be emphasized that the majority of solutions discussed in the literature and describing the temperature distribution in the finger domain are based on the models of the whole human body and they are used to study the thermal response to local cooling, e.g., [7], [21], [24]. The results are presented mainly in the form of temperature on the skin surface of the finger as a function of time. Naturally, research concerning transient problems can be very useful for the analysis of thermal processes proceeding, for example, in the human body sub-domains subjected to the strong external thermal actions (both the high and low ambient temperatures associated with the substantial value of heat transfer coefficient). The analysis of steady state problems (as in the paper presented) is no less important. Temperature field on the skin surface along the finger under typical thermal conditions depends on the blood perfusion rate and metabolic heat source and the apparent differences in rela-

tion to the typical temperature distribution may be indicative of disease states. The quantitative estimation of blood flow rate and heat generation are of great importance for diagnosing blood circulation illness and for the noninvasive measurement of blood glucose [5].

In Fig. 14, the skin surface temperature along the z direction for different values of blood perfusion rate $G_B \rho_B = 0.3$ kg/(m³s) and $G_B \rho_B = 20$ kg/(m³s) is shown. These results are obtained under the assumption that $T_{B10} = 30$ °C, $T_{B2}(0) = 25.5$ °C, $T_B = T_B(z) = 0.5[T_{v1}(z) + T_{v2}(z)]$ (c.f. equations (1), (47)), $\alpha = 7$ W/(m²K) and $T_a = 0$ °C (c.f. equation (5)). For such values it is possible to compare the results with those presented in [25] wherein, among others, the steady-state arterial, venous and skin temperature distributions along the finger are shown. The results presented are slightly different than in [25], because the problem considered here is not axially symmetrical and four arbitrarily placed pairs of artery-vein are taken into account in contrast to the model proposed in [25], [26], where the thermal effects of a pair of blood vessels are included in the model by assuming that they act as two axially temperature-dependent line heat source/sinks, respectively.
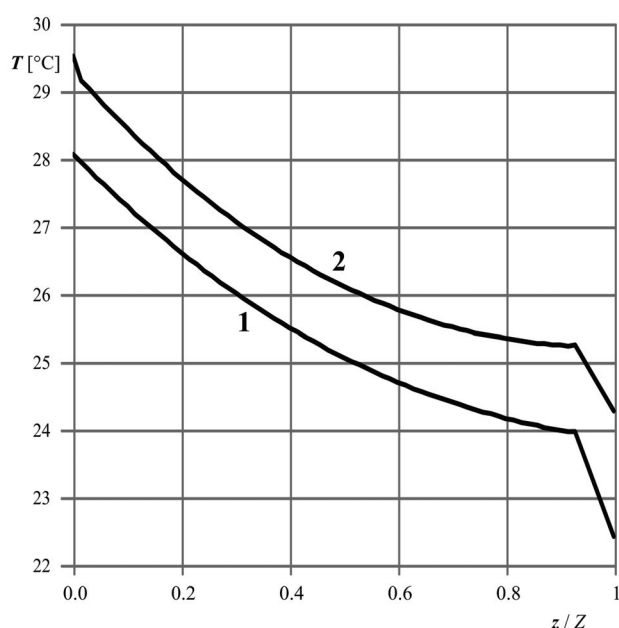

Fig. 14. Temperature distribution on the skin surface along z direction (between the regions of vessels): $1 - G_B \rho_B = 0.3$ kg/(m³s), $2 - G_B \rho_B = 20$ kg/(m³s)

As can be seen in Fig. 14, for the low blood perfusion rate the temperature is lower than in the case of high value of this parameter. Thus, knowledge of the temperature distribution on the surface of the finger allows one to estimate the blood perfusion.

5. Conclusions

The thermal processes proceeding in the domain of the human finger have been considered. The numerical algorithm presented is based on the system of Pennes equations corresponding to the soft and bone tissues and the equations determining the changes of blood temperatures along the vessels (arteries and veins). To solve the problem the algorithm being the composition of the BEM and FDM was developed, while a certain iterative procedure has been introduced. As is well known, the thermal properties of tissue (e.g., thermal conductivity, perfusion coefficient, etc.) are the individual features and may change within a fairly wide range (in other words, they can be treated as the interval numbers [17]). In this paper, the mean values of thermophysical parameters are used and it turned out that the results obtained are quite satisfactory under the condition that the blood temperatures T_{B10} and T_{B20} are chosen properly. In this place the methods of inverse problems solutions can be taken into account, e.g., [10], [14], [19], while the additional information necessary to solve the identification task can result from the knowledge of temperature distribution on the finger surface. Such a problem is currently under investigation. From the medical point of view the identification of blood perfusion rate is of great importance for diagnosing blood circulation illness [5] and this problem can also be solved using the methods of inverse problems solutions. The geometry of the finger domain can be more complex, of course, and the successive layers of the soft tissue (skin, fat, muscle) can be taken into account. It is also possible to use the algorithm proposed for the modeling of thermal processes proceeding in the conditions of low or high ambient temperatures [12], [13] and the big values of heat transfer coefficients. The impact of protective clothing on the temperature field in the domain of the finger can also be analyzed.

References

[1] AVOLIO A.P., *Multi-branched model of the human arterial system*, Med. Biol. Eng. Comput., 1980, Vol. 18, 709–718.

[2] BREBBIA C.A., TELLES J.C.F., WRÓBEL L.C., *Boundary element techniques*, Springer-Verlag, Berlin, New York, 1984.

[3] FIALA D., LOMAS K.J., M. STOHRER M., *Computer predictions of human thermoregulatory and temperature responses to a wide range of environment conditions*, Int. J. Biometeorol., 2001, Vol. 45, 143–159.

[4] FERREIRA M.S., YANAGIHARA J.I., *A transient three-dimensional heat transfer model of the human body*, Int. Commun. Heat Mass., 2009, Vol. 36, 718–724.

[5] He Y., Himeno R., Liu H., Yokota H., Sun Z.G., *Finite element numerical analysis of blood flow and temperature distribution in three-dimensional image-based human finger*, J. Heat Fluid Flow, 2008, Vol. 18(7/8), 932–963.

[6] Huang H.W., Chan C.L., Roemer R.B., *Analytical solutions of Pennes bioheat transfer equation with a blood vessel*, J. Biomech. Eng., 1994, Vol. 116, 208–212.

[7] Karaki W., Ghaddar N., Ghali K., Kuklane K., Holmér I., Vanggaard L., *Human thermal response with improved AVA modeling of the digits*, Int. J. Therm. Sci., 2013, Vol. 67, 41–52.

[8] Majchrzak E., *Application of different variants of the BEM in numerical modeling of bioheat transfer processes*, MCB: Mol Cell Biomech., 2013, Vol. 10(3), 201–232.

[9] Majchrzak E., Mochnacki B., *Numerical model of heat transfer between blood vessel and biological tissue*, CAMES, 1999, Vol. 6, 439–447.

[10] Majchrzak E., Mochnacki B., *Sensitivity analysis and inverse problems in bio-heat transfer modelling*, CAMES, 2006, Vol. 13, 85–108.

[11] Majchrzak E., Mochnacki B., *Numerical modeling of heat transfer between blood vessels (artery and vein) and biological tissue*, IV European Conference on Computational Mechanics, Paris, France, CD-ROM Proceedings, 2009, 1–10.

[12] Majchrzak E., Mochnacki B., Dziewoński M., Jasiński M., *Numerical modelling of hyperthermia and hypothermia processes*, Comp. Mater. Sci., 2011, Vol. 268–270, 257–262.

[13] Majchrzak E., Mochnacki B., Jasiński M., *Numerical modelling of bioheat transfer in multi-layer skin tissue domain subjected to a flash fire*, CFSM, 2003, Vol. 1–2, 1766–1770.

[14] Majchrzak E., Paruch M., *Identification of electromagnetic field parameters assuring the cancer destruction during hyperthermia treatment*, Inverse Probl. Eng., 2011, Vol. 19(1), 45–58.

[15] Majchrzak E., Tarasek D., *Numerical modeling of heat transfer in a single blood vessel and surrounding biological tissue*, Sci. Res. Inst. Math. Comput. Sci. (Czest Univ Technol, Online), 2010, Vol. 2(9), 145–152.

[16] Majchrzak E., Tarasek D., *Numerical analysis of heat transfer in countercurrent blood flow and biological tissue*, Sci. Res. Inst. Math. Comput. Sci. (Czest Univ Technol, Online), 2011, Vol. 2(10), 143–154.

[17] Mochnacki B., Piasecka Belkhayat A., *Numerical modeling of skin tissue heating using the interval finite difference method*, MCB: Mol Cell Biomech., 2013, Vol. 10(3), 233–244.

[18] Nowak A.J., Chapter 3: *Solving linear heat conduction problems by the multiple reciprocity boundary element method*, [in:] *Boundary element methods in heat transfer*, L.C. Wróbel, C.A. Brebbia (eds.), Computational Mechanics Publications, WIT Press, Southampton, Boston, 1992, 63–132.

[19] Paruch M., Majchrzak E., *Identification of tumor region parameters using evolutionary algorithm and multiple reciprocity boundary element method*, Eng. Appl. Artif. Intel., 2007, Vol. 20, 647–655.

[20] Pennes H.H., *Analysis of tissue and arterial blood temperatures in the resting human forearm*, J. Appl. Physiol., 1948, Vol. l, 93–122.

[21] Rida M., Karaki W., Ghaddar N., Ghali K., Hoballah J., *A new mathematical model to simulate AVA cold-induced vasodilatation reaction to local cooling*, Int. J. Biometeorol., 2014, DOI: 10.1007/s00484-014-0792-x.

[22] Salloum M., Ghaddar N., Ghali K., *A new transient bioheat model of the human body and its integration to clothing models*, Int. J. Therm. Sci., 2007, Vol. 46, 371–384.

[23] Schwarz M., Krueger M.W., Busch H.J., Benk Ch., Heilmann C., *Model-based assessment of tissue perfusion and temperature in deep hypothermic patients*, IEEE Trans Biomed. Eng., 2010, Vol. 57, 1577–1586.

[24] Shao H.W., He Y., Mu L.Z., *Numerical analysis of dynamic temperature in response to different levels of reactive hyperemia in a three-dimensional image-based hand model*, Computer Methods in Biomech. Biomed. Engin., 2014, Vol. 17, 865–874.

[25] Shitzer A., Bellomo S., Stroschein L.A., Gonzalez R.R., Pandolf K.B., *Simulation of cold-stressed finger including the effect of wind, gloves, and cold-induced vasodilatation*, J. Biomech. Eng., 1998, Vol. 120, 389–394.

[26] Shitzer A., Stroschein L.A., Vital P., Gonzalez R.R., Pandolf K.B., *Numerical analysis of an extremity in a cold environment including countercurrent arterio-venous heat exchange*, J. Biomech. Eng., 1997, Vol. 119, 179–186.

[27] Stańczyk M., Telega J.J., *Modelling of heat transfer in biomechanics a review*. Part I. *Soft tissues*, Acta Bioeng. Biomech., 2002, Vol. 4(1), 31–61.

[28] Stańczyk M., Telega J.J., *Modelling of heat transfer in biomechanics a review*. Part II. *Orthopaedics*, Acta Bioeng. Biomech., 2002, Vol. 4(2), 3–33.

[29] Stolwijk J.A.J., *Mathematical model of thermoregulation*, Physiological and Behavioral Temperature Regulation, Charles C. Thomas Publishing Company, Illinois, 1970.

[30] Sun X., Eckels S., Zheng Z.C., *An improved thermal model of the human body*, HVAC&R Research, 2012, Vol. 18, 323–338.

[31] Wissler E.H., *Mathematical simulation of human thermal behavior using whole body models*, Heat Mass. Tran. Med. Biol., Plenum Press, New York, 1985.

[32] Xue X., Liu J., *Multi-scale modeling on human intravascular cooling to induce brain hypothermia via circle of Willis*, Forsch Ingenieurwes, 2011, Vol. 75, 257–269.